Supplemental material

Scholz et al., https://doi.org/10.1083/jcb.201806155

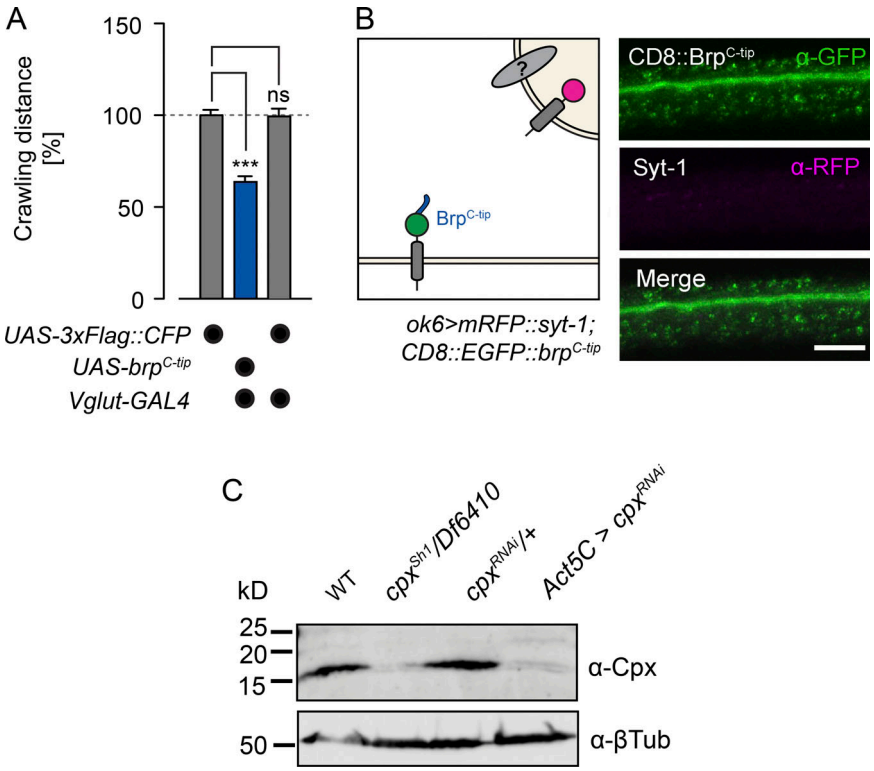

Figure S1. **SV tethering by cytoplasmic Brp$^{C\text{-}tip}$ and Cpx expression levels.** Related to Figs. 1 and 2. **(A)** Quantification of larval crawling distances shows comparable values for *Vglut-GAL4>UAS-3xFlag::CFP* and undriven *UAS-3xFlag::CFP* controls. Thus, the 3xFlag::CFP fusion is not responsible for the effect of Brp$^{C\text{-}tip}$ (*3xFlag::CFP::brp$^{C\text{-}tip}$*). Scores are normalized to *Vglut-GAL4/+*. **(B)** Schematic illustration (left) and confocal images (right) of motor axons expressing CD8::EGFP::Brp$^{C\text{-}tip}$ (*ok6-GAL4>UAS-CD8::EGFP::brp$^{C\text{-}tip}$*). Membrane-attached Brp$^{C\text{-}tip}$ does not capture SVs at ectopic sites. **(C)** The *cpx^{RNAi}* strain employed in the screen for Brp interactors reduces *cpx* expression. Western blot analysis using a polyclonal antibody against Cpx (Huntwork and Littleton, 2007) shows the absence and reduction of Cpx protein levels (~20-kD band) in *cpx^{Sh1}/Df6410* and *Actin-5C-GAL4>UAS-cpx^{RNAi}* animals, respectively. β-tubulin served as loading control. Data presented as mean ± SEM ($n \geq 19$; Table S1). ***, $P \leq 0.001$ (rank sum test). Scale bar: 5 µm. ns, not significant.

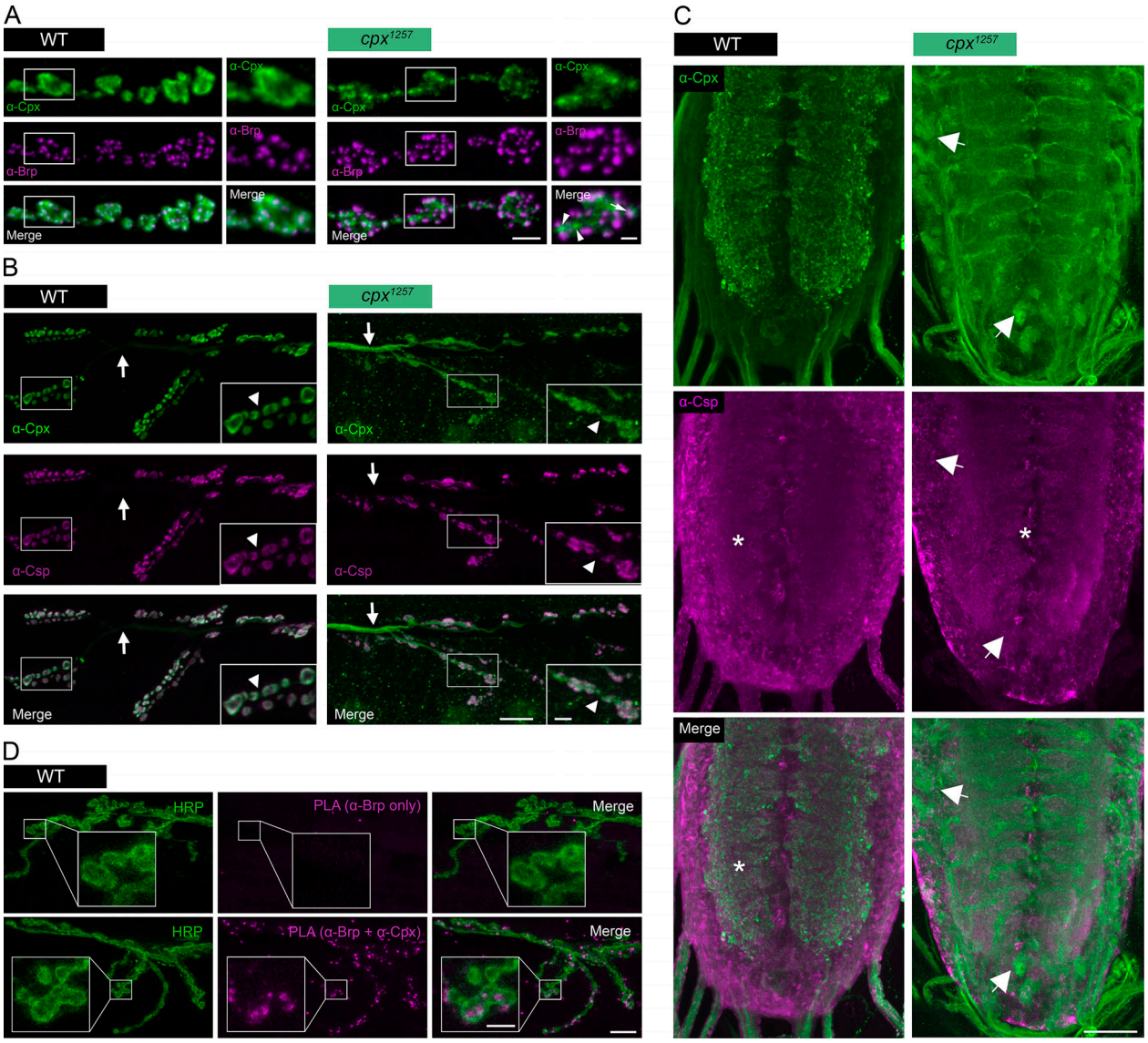

Figure S2. **Disrupted farnesylation alters the subcellular distribution of Cpx.** Related to Fig. 2. **(A)** Cpx forms clusters at *cpx*^{1257} mutant NMJs. Costaining against Cpx (green) and Brp (magenta) at WT and *cpx*^{1257} NMJs. In the mutant, Cpx forms clusters, which are not visible in the WT and only partially overlap with active zones (arrow, colocalization with Brp; arrowheads, no overlap). **(B)** Costaining against Cpx (green) and CSP (magenta) shows disturbed colocalization of Cpx with SVs at *cpx*^{1257} NMJs. Here, Cpx is distributed throughout motor axons (arrows) and interbouton sections (arrowheads) and no longer displays the characteristic enrichment in the bouton cortex. **(C)** Whereas Cpx is prominent in synapse-rich regions of the WT VNC, Cpx is mainly found in somata of *cpx*^{1257} mutants (arrows). Asterisks mark the neuropil. **(D)** PLA. Maximal projections of confocal images showing that Brp and Cpx are located within ∼40 nm of each other at WT larval NMJs (lower row). Colocalization via PLA (magenta) was determined using primary antibodies against Brp and Cpx. Neuronal membranes were visualized with an antibody against HRP (green). To control the specificity of Brp–Cpx complexes, samples were incubated with the Brp antibody only (upper row). Scale bars: (A) 3 µm, inset 1 µm; (B and D) 10 µm, inset 3 µm; and (C) 30 µm.

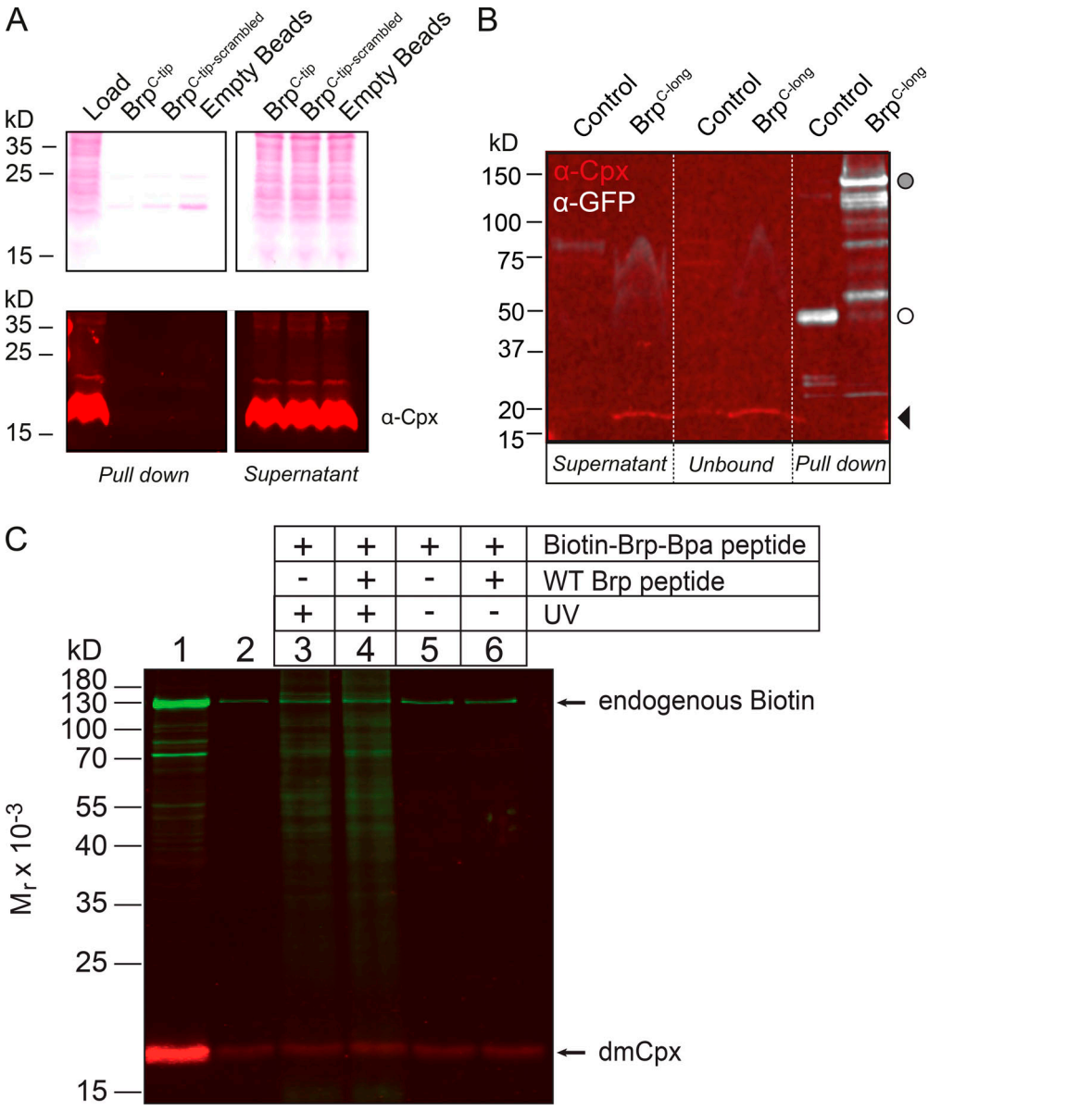

Figure S3. **The interaction between Cpx and Brp escapes biochemical capture.** Related to Fig. 4. **(A)** A synthetic peptide including Brp$^{C\text{-}tip}$ was immobilized to generate an affinity matrix for capturing Cpx. A Brp$^{C\text{-}tip}$ variant with randomly scrambled amino acid sequence and empty agarose beads served as controls. Upper panel: Ponceau-S staining. Lower panel: Cpx immunoblot. Supernatant indicates unbound protein, pull down shows Cpx (~18-kD band) in the protein input suggesting sufficient protein extraction. Cpx was not found in the eluate from the affinity matrix containing Brp$^{C\text{-}tip}$. **(B)** Western blot analysis of mCD8::EGFP (Control) and mCD8::EGFP::Brp$^{C\text{-}long}$ (Brp$^{C\text{-}long}$) protein complexes immobilized using GFP-tagged magnetic beads. An ~18-kD Cpx band was detected in supernatant and unbound fractions using a rb-α-Cpx antibody (red, arrowhead). However, while mCD8::EGFP (~50 kD, white circle) and mCD8::EGFP::Brp$^{C\text{-}long}$ (~150 kD, gray circle) signals indicate sufficient capture of Cpx bait, Cpx itself was not detected in pull-down samples. **(C)** Photoaffinity labeling of proteins in fly head homogenate with Biotin-Brp-Bpa peptide. Supernatant 2 (10 mg/ml protein, lane 1) was used at a final protein concentration of 0.1 mg/ml (see lane 2 for comparison) in the respective photoreactions. Fly head homogenate was incubated with Biotin-Brp-Bpa peptide (lanes 3–6) in the absence (lanes 3 and 5) or presence (lanes 4 and 6) of an excess of WT Brp peptide, the latter used as competitor to show the specificity of a potentially appearing photoadduct. Samples processed in parallel, but without exposure to UV irradiation served as controls. In the case of a capture of the Cpx–Brp interaction as covalent photoadduct, a signal codetected by α-Cpx antibodies and streptavidin was expected at ~20 kD (i.e., the size of dmCpx + Biotin-Brp-Bpa peptide) in lane 3 but was not apparent. Neither an increase in protein input (1 mg/ml final concentration) nor in Biotin-Brp-Bpa peptide (100 µM final concentration) led to a positive result (data not shown). Note that further positive controls for on-blot biotin detection were performed successfully (Biotin-BSA, Thermo Fisher Scientific; Biotin-Brp-Bpa peptide) but are not shown in this representative image.

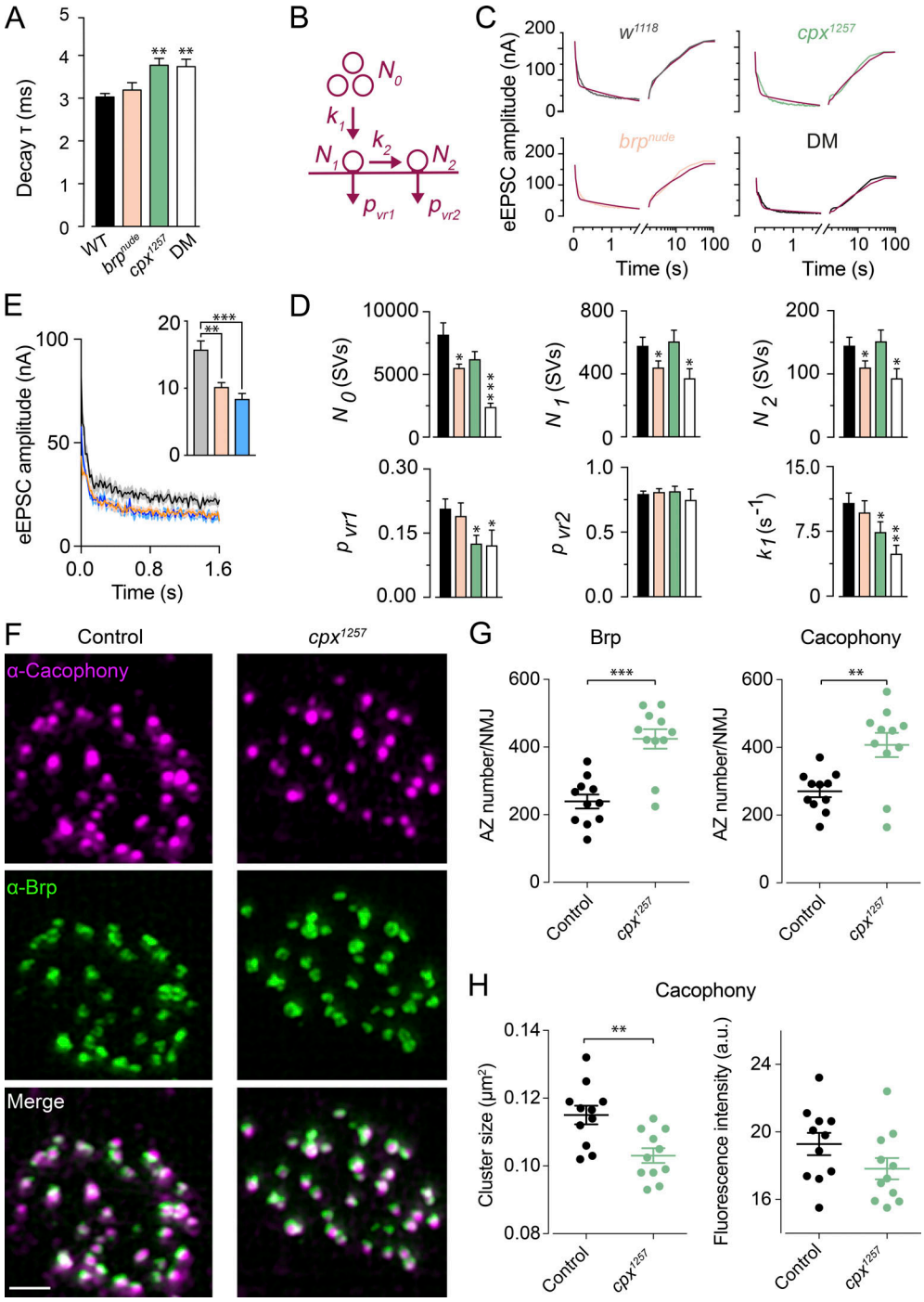

Figure S4. **Additional electrophysiology and imaging of *cpx*^{1257} active zones.** Related to Fig. 5. **(A)** The decay time constant (τ) of eEPSCs is unaltered in *brp*^{nude} single mutants and prolonged in *cpx*^{1257} animals and DMs ($n \geq 10$, *t* test; Table S7). This indicates that pronounced receptor desensitization does not contribute to the mutants' electrophysiological phenotypes. **(B)** Modeling short-term plasticity. Individual experiments (60-Hz train plus recovery in 1.5 mM $[Ca^{2+}]_e$; $n \geq 9$) were fitted with a model containing two pools of RRVs (N_1, N_2) with different release probabilities (p_{vr1}, p_{vr2}), which are refilled (k_1, reloading rate $[s^{-1}]$) from a finite supply pool (N_0, likely corresponding to SVs attached to the T-bar; Hallermann et al., 2010a). **(C)** Example fits to average data. **(D)** The model predicts different SV reloading defects in the single mutants (significantly smaller N_0 in *brp*^{nude}, lower k_1 in *cpx*^{1257}). Importantly, the DM displays a sum of phenotypes: additive reduction of N_0 and k_1, p_{vr1} similar to *cpx*^{1257} and RRV pools comparable to *brp*^{nude} (note difference to estimates in Fig. 5 I; rank sum test versus WT for p_{vr1} *brp*^{nude} and DM, p_{vr2} DM, k_1 *brp*^{nude}, *t* test for all others). **(E)** Epistasis assay. Average eEPSC amplitudes at 60-Hz stimulation (1 mM $[Ca^{2+}]_e$; light shading shows SEM) and quantification of steady-state level (last 10 eEPSCs measured manually; gray: *ok6-GAL4/+*, beige: *brp*^{nude}*/brp*^{69}*,ok6-GAL4*, blue: *brp*^{nude}*/brp*^{69}*,ok6-GAL4;UAS-EGFP::cpx/+*; $n \geq 8$, rank sum test; Table S7). **(F)** A GFP-tagged version of Cacophony, an α1 subunit of voltage-gated Ca^{2+} channels (Kawasaki et al., 2004; Kittel et al., 2006), was expressed in larval motoneurons (*ok6-GAL4>UAS-cac*^{GFP}) and visualized by SIM. Examples show stainings against GFP (magenta) and Brp (mAb nc82, green). **(G and H)** Quantification of imaging data from muscle 4 shows an increased number of Cacophony clusters (*t* test) and Brp-positive active zones (rank sum test) in *cpx*^{1257} mutants. Whereas their signal intensity is unaltered, the average size of Cacophony clusters is significantly reduced in *cpx*^{1257} mutants ($n = 11$, *t* test; Table S10). Data are presented as mean ± SEM. *, P ≤ 0.05; **, P ≤ 0.01; ***, P ≤ 0.001. Scale bar: 1 µm.

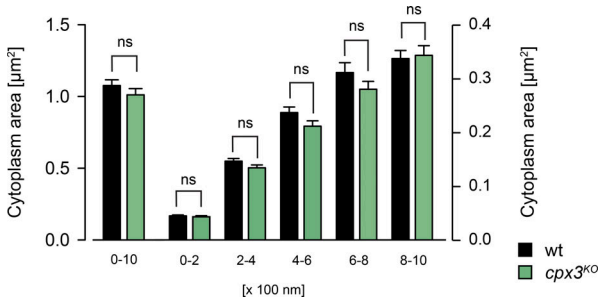

Figure S5. **Ribbons of *cpx3*^{KO} RB terminals are surrounded by a normal cytoplasmic space.** Related to Fig. 6. Analysis of electron micrographs of WT (black) and *cpx3*^{KO} (green) RB terminals. Quantification of the cytoplasmic area surrounding synaptic ribbons within five 200-nm-thick concentric shells (right axis) and in sum (left axis, 0–1,000 nm). Data are presented as mean ± SEM ($n \geq 46$, rank sum test; Table S11). ns, not significant.

Table S1. Crawling distance

Genotype	Crawling distance (cm/min)	n	P
Related to Figure 1D			
w^{1118};;;	7.52 ± .30	25	-
w^{1118}; brp^{nude}/brp^{69};;	6.01 ± .15	25	< .0001
w^{1118}; UAS-$brp^{C\text{-}tip}$/+;;	8.66 ± .57	18	< .0001
w^{1118}; ok6-GAL4/+;;	7.35 ± .29	20	.0001
w^{1118}; ok6-GAL4/UAS-$brp^{C\text{-}tip}$;;	5.41 ± .35	21	-
			t-test

Related to Figure S1			
w^{1118} Vglut/+;;;	7.78 ± .31	19	-
w^{1118} Vglut/+; UAS-$brp^{C\text{-}tip}$;;	4.81 ± .24	28	< .0001
w^{1118}Vglut/+; UAS-CFP;;	7.17 ± .31	20	.2011
			Rank sum test

Related to Figure 3A			
w^{1118};;;	7.74 ± .40	21	-
w^{1118}; brp^{nude}/brp^{69};;	5.80 ± .30	22	.0003 .0004
w^{*};; cpx^{1257}/cpx^{Sh1};	4.14 ± .14	25	<.0001 .3894
w^{1118}; brp^{nude}/brp^{69}; cpx^{1257}/cpx^{Sh1};	4.34 ± .20	19	<.0001
			t-test

Related to Figure 3B			
w^{1118};;;	7.10 ± .25	36	-
w^{1118};brp^{nude}/+;;	8.24 ± .28	31	.0039 <.0001
w^{*};;cpx^{Sh1}/+;	6.75 ± .27	37	.3343 .0012
w^{1118};brp^{nude}/+;cpx^{Sh1}/+;	5.03 ± .37	27	.0001
w^{1118};brp^{69}/+;;	7.92 ± .29	30	.0353 <.0001
w^{*};;cpx^{1257}/+;	7.39 ± .32	29	.7766 .0039
w^{1118};brp^{69}/+;cpx^{1257}/+;	5.58 ± .37	30	.0062
			Rank sum test

Values represent the mean ± SEM, *n* denotes number of larvae. P values in gray and black indicate comparisons with genetic controls and between experimental groups, respectively (as indicated in the figures).

Table S2. Quantification of paired-pulse ratios (PPR) following Brp$^{C\text{-}tip}$ expression

Genotype	PPR					
Related to Figure 1 E						
	10 ms	**30 ms**	**100 ms**	**300 ms**	**1,000 ms**	***n***
w^{1118};ok6-GAL4/+;;	0.94 ± .03	0.98 ± .02	0.95 ± .02	0.92 ± .01	0.95 ± .01	12
w^{1118};ok6-GAL4/UAS-brp$^{C\text{-}tip}$;;	0.85 ± .04 (.0783)	0.93 ± .02 (.0351)	0.90 ± .02 (.0120)	0.90 ± .01 (.3123)	0.93 ± .01 (.2145)	12
w^{1118};brp^{nude},ok6-GAL4/brp^{69};;	0.82 ± .01 (.0014)	0.89 ± .02 (.0086)	0.87 ± .01 (.0003)	0.87 ± .01 (.0004)	0.91 ± .01 (.0004)	12
Rank sum test, P values are given in parentheses						

Data are presented as mean ± SEM; *n* denotes number of NMJs. P values (given in parentheses) indicate comparisons with the control (*w^{1118};ok6-GAL4/+;;*).

Table S3. Candidates for the genetic screen.

Functional involvement	Symbol	Protein name	Off-targets	Chromosome	VDRC stock
Related to Figure 2A					
Priming/ regulation	*dunc-13*	dunc-13	0	2	*v33606*
	tomosyn	tomosyn	0	3	*v43629*
	cpx	complexin	0	3	*v21477*
Fusion/Ca^{2+}-sensing	*dCirl*	Ca^{2+}-independent receptor of latrotoxin	110	2	*v29969*
	dCAPS	CAPS	0	2	*v25291*
	csp	Cysteine string protein	1	2	*v103201*
	syt-12	Synaptotagmin-12	0	2	*V47506*
	syt-7	Synaptotagmin-7	0	3	*v24988*
Regulators, effectors & Rabs	*rim-1*	Rab3-interacting molecule	0	2	*v39384*
	rab3-GAP	rab3 GTPase binding protein	0	3	*v27824*
	gdi	GDP dissociation inhibitor	1	3	*v26537*
	rph	Rabphilin	15	2	*v52438*
	rac-1		1	1	*v49247*
	rab5	Rab3-binding protein 5	3	2	*v34094*
SV phospho-proteins	*sng-1*	Synaptogyrin	0	3	*v8784*
	syn	Synapsin	0	2	*v110606*
Endocytosis	*AnnB9*	AnnexinB9	2	2	*v27493*
	AnnB10	AnnexinB10	0	2	*v36107*
	twf	Twinfilin	0	2	*v25817*
Others	*dysb*	Dysbindin	0	2	*v34354*
	atg-1	Autophagy-specific gene 1	0	2	*v16133*
	rsk	Ribosomal S6 kinase	14	3	*v5702*
	sap47	Synapse-associated proteine 47 kDa	0	2	*v35445*
	dsyd-1	Sunday driver-1	0	2	*v35346*
	dvglut	Vesicular glutamat transporter	0	3	*v2574*
	vti1a	Vesicle transport through interaction with t-SNAREs homolog 1A	0	3	*v45726*
	Mctp	Multiple-C2-domain TM proteins	0	3	*v10061*

List of 27 different genes tested in the RNAi-based screen. The gene products are involved in different steps of the SV cycle.

Table S4. Imaging basis to screen for Brp interactors

Genotype	SYT mean intensity axon/NMJ (a.u.)	*n*	P
Related to Figure 2 F			
w^{1118};ok6-GAL4,mRFP::syt-1/+;no brp;	0.59 ± .04	17	-
w^{1118};ok6-GAL4,mRFP::syt-1/+;$brp^{C\text{-}long}$/+;	0.78 ± .06	16	.0267
w^{1118};ok6-GAL4,mRFP::syt-1/+;$brp^{C\text{-}long}$/$brp^{C\text{-}tip}$;	0.59 ± .08	16	.0302
w^{1118};ok6-GAL4,mRFP::syt-1/+;no brp/cpx^{v21477};	0.31 ± .02	22	-
w^{1118};ok6-GAL4,mRFP::syt-1/+;$brp^{C\text{-}long}$/cpx^{v21477};	0.31 ± .03	22	.6221
w^{1118};ok6-GAL4,mRFP::syt-1/+;cpx^{1257}/cpx^{Sh1};	0.55 ± .07	13	-
w^{1118};ok6-GAL4,mRFP::syt-1/+;$brp^{C\text{-}long}$,cpx^{1257}/cpx^{Sh1};	0.44 ± .04	21	.1108
			Rank sum test

SV distributions (axon/NMJ ratio) in wt (white), $cpx^{v12477(RNAi)}$ (light green) and cpx^{1257} (dark green) genetic backgrounds. Values represent the mean ± SEM, *n* denotes number of larvae. P values in gray and black indicate comparisons with genetic controls and between experimental groups, respectively.

Table S5. Quantification of SV numbers at NMJ T-bars

Genotype	Number of SVs/T-bar				
Related to Figure 4 B					
	50-100 nm	**100-150 nm**	**150-200 nm**	**200-250 nm**	***n***
$w^{1118};;;$	6.0 ± .19	8.14 ± .28	8.93 ± .43	11.76 ± .54	58
$w^{1118};brp^{nude}/brp^{69};;$	3.40 ± .22 (<.0001) (.8933)	5.36 ± .26 (<.0001) (.8407)	6.92 ± .29 (.0004) (.1143)	10.62 ± .48 (.0700) (.5105)	42
$w^{*};;cpx^{1257}/cpx^{Sh1};$	4.52 ± .22 (<.0001) (.0034)	5.80 ± .20 (<.0001) (.1553)	6.91 ± .27 (.0001) (.1052)	10.64 ± .43 (.0732) (.4081)	65
$w^{1118};brp^{nude}/brp^{69};cpx^{1257}/cpx^{Sh1};$	3.50 ± .22 (<.0001)	5.24 ± .27 (<.0001)	6.24 ± .37 (<.0001)	10.11 ± .60 (.0325)	38
Rank sum test, P values are given in parentheses					

Values represent the mean ± SEM; *n* denotes number of T-bars. P values in gray and black indicate comparisons with WT and the DM, respectively.

Table S6. *d*STORM analysis of the CAZ ultrastructure

Genotype	CAZ area (µm²)	P	Localizations/CAZ	P	*n*
Related to Figure 4C					
w^{1118};;;	0.09 ± .003	-	556.39 ± 48.81	-	19
w^{1118};brp^{nude}/brp^{69};;	0.07 ± .002	.0002	552.89 ± 42.19	1.00	21
w^{*};; cpx^{1257}/cpx^{Sh1};	0.08 ± .003	.0507	534.57 ± 53.19	.8673	18
w^{1118};brp^{nude}/brp^{69};cpx^{1257}/cpx^{Sh1};	0.08 ± .002	.0016	578.37 ± 51.19	.8331	20
		t-test		Rank sum test	

Data are represented as mean ± SEM; *n* denotes number of NMJs. P values indicate comparisons with WT.

Table S7. Electrophysiological analysis of mutant NMJs

Genotype	eEPSC amplitude (-nA)	P	*n*	Mini frequency (Hz)	P	*n*
	Related to Figure 5 E			Related to Figure 5 B		
$w^{1118};;;$	44.80 ± 3.02	-	10	1.11 ± .18	-	15
$w^{1118};brp^{nude}/brp^{69};;$	50.50 ± 5.05	.3800 .5924	13	0.83 ± .05	.4450 < .0001	14
$w^{*};;cpx^{1257}/cpx^{Sh1};$	52.77 ± 2.28	.0431 .1858	13	62.60 ± 5.91	< .0001 < .0001	14
$w^{1118};brp^{nude}/brp^{69};cpx^{1257}/cpx^{Sh1};$	47.09 ± 3.57	.6374	12	23.19 ± 2.52	< .0001	14
		t test			Rank sum test	

Genotype	PPR (1 mM Ca^{2+})					
	Related to Figure 5 G					
	10 ms	**30 ms**	**100 ms**	**300 ms**	**1,000 ms**	***n***
$w^{1118};;;$	1.50 ± .10	1.51 ± .11	1.19 ± .04	1.05 ± .02	0.99 ± .01	10
$w^{1118};brp^{nude}/brp^{69};;$	1.08 ± .07 (.0039)	1.21 ± .04 (.0101)	0.97 ± .02 (.0200)	1.01 ± .02 (.1138)	0.98 ± .01 (.4757)	13
$w^{*};;cpx^{1257}/cpx^{Sh1};$	1.03 ± .03 (.0009)	1.05 ± .03 (.0002)	0.98 ± .02 (.0006)	0.94 ± .02 (.0006)	0.96 ± .01 (.0586)	13
$w^{1118};brp^{nude}/brp^{69};cpx^{1257}/cpx^{Sh1};$	0.80 ± .06 (.0002)	0.90 ± .04 (.0001)	0.85 ± .02 (.0001)	0.87 ± .02 (.0001)	0.91 ± .01 (.0011)	12
	Rank sum test, P values are given in parentheses					

Genotype	PPR (0.6 mM Ca^{2+})					
	Related to Figure 5 G					
	10 ms	**30 ms**	**100 ms**	**300 ms**	**1,000 ms**	***n***
$w^{1118};;;$	1.81 ± .09	1.62 ± .08	1.30 ± .05	1.12 ± .05	0.10 ± .03	14
$w^{1118};brp^{nude}/brp^{69};;$	1.58 ± .09 (.0769)	1.45 ± .08 (.1354)	1.24 ± .07 (.1238)	1.18 ± .03 (.0565)	1.00 ± .02 (.9817)	14
$w^{*};;cpx^{1257}/cpx^{Sh1};$	1.44 ± .09 (.0123)	1.27 ± .09 (.0019)	1.07 ± .03 (.0026)	1.07 ± .05 (.1354)	0.98 ± .02 (.8362)	14
$w^{1118};brp^{nude}/brp^{69};cpx^{1257}/cpx^{Sh1};$	1.25 ± .07 (.0004)	1.15 ± .05 (.0002)	1.00 ± .02 (.0005)	0.94 ± .02 (.0013)	0.95 ± .02 (.4520)	13
	Rank sum test, P values are given in parentheses					

Genotype	eEPSC decay τ (ms)	P	*n*
	Related to Figure S4		
$w^{1118};;;$	3.03 ± 0.08	-	10
$w^{1118};brp^{nude}/brp^{69};;$	3.19 ± 0.17	.4462	13
$w^{*};;cpx^{1257}/cpx^{Sh1};$	3.77 ± 0.16	.0011	13
$w^{1118};brp^{nude}/brp^{69};cpx^{1257}/cpx^{Sh1};$	3.74 ± 0.17	.0022	12
		t test	

Genotype	eEPSC steady-state level (-nA; last 10 events)	P	n
Related to Figure 5H			
$w^{1118};;;$	51.76 ± 0.40	-	9
$w^{1118};brp^{nude}/brp^{69};;$	27.22 ± 0.57	< .0001 < .0001	13
$w^{*};;cpx^{1257}/cpx^{Sh1};$	29.66 ± 0.28	< .0001 < .0001	13
$w^{1118};brp^{nude}/brp^{69};cpx^{1257}/cpx^{Sh1};$	14.46 ± 0.27	< .0001	12
		t-test	

Related to Figure S4			
$w^{*};ok6\text{-}GAL4/+;;$	15.74 ± 1.3	-	9
$w^{*};brp^{nude}/brp^{69}$, ok6-GAL4;;	10.17 ± 0.67	.0055	8
$w^{*};brp^{nude}/brp^{69}$, ok6-GAL4;UAS-EGFP::cpx/+;	8.4 ± 0.82	.0010	10
		Rank sum test	

Data are presented as mean ± SEM; *n* denotes the number of NMJs. P values in gray and black indicate comparisons with WT and the DM, respectively.

Table S8. **Quantification of AZ numbers**

Genotype	AZ number	P	*n*
Related to Figure 5 C			
$w^{1118};;;$	414.06 ± 26.59	-	16
$w^{1118};brp^{nude}/brp^{69};;$	352.50 ± 26.42	.1683 .8968	8
$w^{*};;cpx^{1257}/cpx^{Sh1};$	523.78 ± 32.16	.0138 .0133	9
$w^{1118};brp^{nude}/brp^{69};cpx^{1257}/cpx^{Sh1};$	369.10 ± 27.64	.2357	10
		Rank sum test	

Data are represented as mean ± SEM; *n* denotes number of NMJs. P values in gray and black indicate comparisons with WT and the DM, respectively.

Table S9. Back extrapolation of cumulatively plotted eEPSC amplitudes

Genotype	Cumulative eEPSC amplitude (nA)	P	*n*
Related to Figure 5 I			
$w^{1118};;;$	205.77 ± 39.10	-	9
$w^{1118};brp^{nude}/brp^{69};;$	242.66 ± 32.58	.4771 .2442	13
$w^{*};;cpx^{1257}/cpx^{Sh1};$	335.59 ± 37.10	.0292 .0032	13
$w^{1118};brp^{nude}/brp^{69};cpx^{1257}/cpx^{Sh1};$	197.72 ± 16.80	.8380	12
		t-test	

Estimates of average RRV pool sizes using linear fits to 0.3–0.5 s (upper table) to the stimulus train. Data are presented as mean ± SEM; *n* denotes number of NMJs. P values in gray and black indicate comparisons with WT and the DM, respectively.

Table S10. Quantification of Ca^{2+} channel clusters at *cpx*^{1257} active zones

Genotype	Brp cluster #	P	*n*	Cacophony cluster #	P	*n*
Related to Figure S4						
w**; UAS-cac1::EGFP ok6-GAL4/+;;*	239 ± 21	-	11	270 ± 17	-	11
w**; UAS-cac1::EGFP ok6-GAL4/+; cpx*^{1257}*/cpx*^{sh1}*;*	424 ± 29	.0006	11	407 ± 36	.0026	11
		Rank sum test			*t* test	

Genotype	Cacophony cluster size (μm^2)	P	*n*	Cacophony cluster intensity (a.u.)	P	*n*
Related to Figure S4						
w**; UAS-cac1::EGFP ok6-GAL4/+;;*	.115 ± .002	-	11	19.29 ± .66	-	11
w**; UAS-cac1::EGFP ok6-GAL4/+; cpx*^{1257}*/cpx*^{sh1}*;*	.103 ± .002	.0027	11	17.83 ± .63	.1261	11
		t test			*t*test	

Data are presented as mean ± SEM; *n* denotes number of NMJs.

Table S11. **Analysis of synaptic ribbons at mouse RB terminals**

Genotype	SV numbers/200 nm shell					
Related to Figure 6C						
	0-200 nm	**200-400 nm**	**400-600 nm**	**600-800 nm**	**800-1,000 nm**	***n***
wt	4.76 ± .34	17.00 ± 1.01	26.83 ± 1.83	29.91 ± 2.10	34.48 ± 2.36	46
cpx3^{KO}	3.00 ± .22 (.0001)	13.44 ± 0.74 (.0042)	22.42 ± 1.62 (.1069)	27.46 ± 1.77 (.3987)	33.60 ± 2.12 (.8589)	48
Rank sum test, P values are given in brackets						

Genotype	Cytoplasm area (µm^2)/200 nm shell					
Related to Figure S5						
	0-200 nm	**200-400 nm**	**400-600 nm**	**600-800 nm**	**800-1,000 nm**	***n***
wt	0.05 ± .002	0.15 ± .005	0.24 ± .010	0.31 ± .018	0.34 ± .015	46
cpx3^{KO}	0.04 ± .002 (.2515)	0.13 ± .005 (.0581)	0.21 ± .010 (.1433)	0.28 ± .015 (.3311)	0.34 ± .018 (.8264)	48
Rank sum test, P values are given in brackets						

Data are represented as mean ± SEM; *n* denotes number of ribbons. P values indicate comparisons with WT.